Coherence dynamics of excitons and continuum excitations in InP

G. R. Allan and H. M. van Driel
Department of Physics, University of Toronto, Toronto, Canada, M5S 1A7
(Received 20 February 1998; revised manuscript received 30 October 1998)

The coherent response of excitons and low-energy continuum excitations has been determined in InP at 5 K using spectrally resolved four-wave mixing employing 40 fs pulses in a self-diffraction geometry. The excitons were studied under simultaneous excitation with free carriers of density $10^{15}<N<10^{17}$ cm^{-3}. Excellent agreement between experiment and a simple theory based on excitation induced dephasing is obtained for an exciton dephasing rate which varies as N^{α} with $\alpha\approx 0.5$ in the density range. The sublinear dependence is suggestive of carrier-exciton screening effects; however, a variation in exciton oscillator strength and/or phase-space filling effects may also be contributing to the density dependence of the four-wave-mixing signal. For the continuum excitations we spectrally resolve the influence of LO phonons on continuum dephasing. Below the threshold for LO-phonon emission by electrons we determine a dephasing rate of ~ 8 ps^{-1} at $N=5\times 10^{16}$ cm^{-3}; for states just above the threshold for LO-phonon emission, the dephasing rate is >13 ps^{-1}, our resolution limit. [S0163-1829(99)06024-5]

I. INTRODUCTION

The coherent dynamics of carriers in semiconductors has been extensively investigated during the past decade.[1,2] Since the pioneering work of Schultheis *et al.*,[3] who observed the coherent response of excitons in GaAs, degenerate four-wave mixing (FWM) has become the technique of choice to investigate coherent exciton and continuum dynamics. Much of that research has focused on excitons in both bulk and quantum-well structures, because the dephasing time of excitons is typically 1 ps and the coherent dynamics can be easily resolved with nominally 100-fs pulses.[4–12] Exciton-exciton interactions (i.e., many-body effects) have been demonstrated to have a strong influence on exciton dynamics. Relatively few experiments have investigated the effects of exciton-continuum interactions on coherent exciton dynamics, although, since the work of Schultheis *et al.* it has been known that the dephasing rate of excitons increases substantially in the presence of free carriers due to exciton-carrier scattering. Recently, experiments have been performed with such short optical pulses that it is possible to excite mutually coherent excitons and continuum excitations simultaneously with the same pulse.[13–19] Under such conditions the exciton dynamics appear to be significantly different than that observed by Schultheis *et al.*, which were obtained with narrower bandwidth excitation and an incoherent free-carrier population. The intriguing feature of the exciton dynamics is an apparent violation of the uncertainty principle: the FWM coherent emission is spectrally narrower than the excitation pulse yet occurs only for temporally overlapped excitation pulses.

Within the context of the semiconductor Bloch equations (SBE),[20] if the exciton dephasing time is independent of density one expects a coherent interaction to produce emission for pulse separations up to the exciton coherence time which is related to the inverse of the linewidth. An explanation for the apparent violation of the uncertainty principle has been discussed in terms of a model for exciton-continuum interactions, which is referred to as excitation-induced dephasing (EID).[21,18] EID was originally proposed to explain effects of exciton-exciton interactions on exciton dynamics,[22] and it was shown that screening plays a role in determining the density dependence of the dephasing. For EID involving exciton-free carrier interations, this model has been primarily used to explain results qualitatively.[17–19] The EID mechanism appears to be most important at low excitation density,[17,23] although this has not yet been explained adequately by the simple EID model.

In this paper, we present results of spectrally resolved (SR) and spectrally integrated (SI-) FWM experiments which investigated both exciton and continuum dephasing dynamics in InP at 5 K following excitation by 30–50-fs pulses centered at 1.46 eV. In particular, exciton FWM experiments have been conducted as a function of free-carrier density, and analyzed in terms of the density dependence of EID. In many previous analyses of exciton EID results, the exciton-carrier scattering rate was assumed to be linearly dependent on excitation density, but we find that as the free-carrier density is increased from 10^{15} to 5×10^{16} cm^{-3}, a sublinear (approximately square root) variation is observed, possibly reflecting screening effects on exciton-carrier interacitons as well as exciton oscillator strength.

We also report results on the dephasing of near-band-edge continuum states. Compared to excitons, little is known about the dephasing mechanisms of continuum excitations, ostensibly because the dephasing times are typically tens of femtoseconds or less and are difficult to resolve temporally.[13,18,24–27] The first measurements[24] of continuum dephasing rates in a semiconductor were carried out on GaAs with 620-nm pulses of 6-fs duration. These pulses excited continuum states with energies of the order of several hundred meV and over a bandwidth of ~ 200 meV. Dephasing was assigned to screened carrier-carrier interactions, and occurred on a time scale near the pulse resolution limit. The authors reported that the dephasing rate varied with free-carrier density N as $N^{0.3}$. Since the energy of an electron or hole state determines whether certain phonon emission events, including those involving intervalley transfer, can oc-

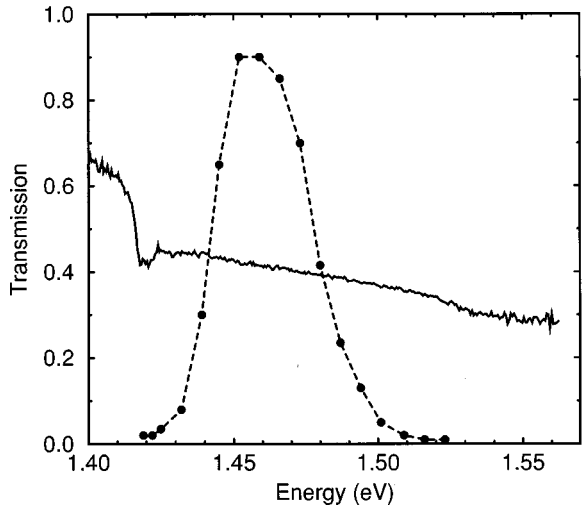

FIG. 1. Transmission spectrum of 0.3-μm-thick InP sample at 5 K (solid line). A typical spectrum of laser pulses used in the FWM experiments is also shown (circles).

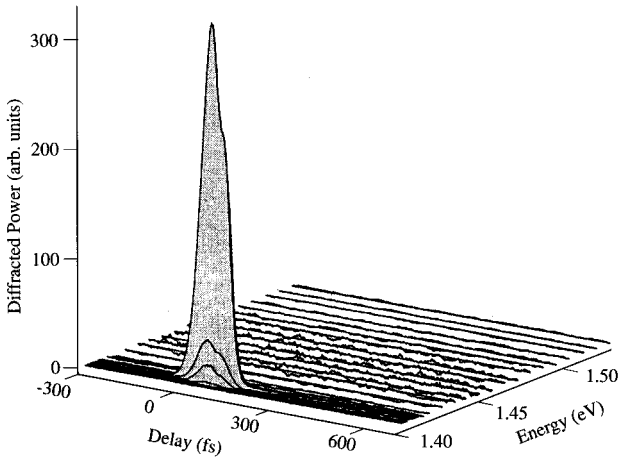

FIG. 2. FWM spectrum vs delay for excitation at 1.46 eV, and a carrier density of 1×10^{15} cm^{-3}.

cur, it is not clear that all states within such a large excitation bandwidth should have the same dephasing rate. Indeed, experiments have now shown that the continuum dephasing rate is affected by several scattering channels.[15,25] However, to our knowledge the effect of a simple mechanism such as phonon emission on continuum dephasing has not been spectrally resolved.

In Sec. II we give details of the experiments. This is followed in Sec. III by results and discussion of FWM experiments. In Sec. III A we compare the exciton dynamics to predictions of an EID model with a density dependence of the exciton-carrier scattering rate. In Sec. III B the continuum dephasing rate is investigated over a range of energy which allows us to discern the onset of LO-phonon emission by electrons. Section IV summarizes our results.

II. EXPERIMENTAL DETAILS

The SR- and SI-FWM experiments were performed in a self-diffraction geometry on a 0.3-μm-thick sample of intrinsic InP. A heterostructure consisting of the thin InP layer and a 0.5-μm stop-etch layer of $In_xGa_{1-x}As$ was grown on an InP(100) substrate. The InP film was isolated from the heterostructure by performing a two-step chemical etch procedure that first removed the InP substrate and then removed the stop-etch layer.[28] The film was van der Waals bonded to a sapphire substrate and held at 5 K. The band gap of InP at 5 K is 1.42 eV, and the exciton binding energy is 5 meV.[29] The experiments employed a mode-locked Ti:sapphire laser producing $\sim$40-fs pulses tunable from 1.46 to 1.55 eV. Figure 1 shows a low-resolution (3 meV) transmission spectrum of the InP sample (taken with a white light source) and the laser spectrum. In a degenerate FWM experiment, the laser beam is split into two approximately equal amplitude beams, with wave vectors $\mathbf{K}_1$ and $\mathbf{K}_2$, which are focused onto the sample by the same lens ($f=50$ cm). The FWM signal diffracted into the direction $\mathbf{2K}_2-\mathbf{K}_1$ is spectrally resolved with a monochromator (1.3-meV resolution) and detected with a photomultiplier tube. The diffracted spectrum is measured as a function of time delay τ between the two pulses.

To investigate the EID diffraction mechanism, the exciton density was intentionally kept very low by tuning the laser to 1.46 eV, which is well above the exciton resonance. Therefore FWM diffraction mechanisms that are nonlinear in exciton density (e.g., free-induction decay and local-field effects based on exciton-exciton interactions) should be much weaker than the EID mechanism.

III. RESULTS AND DISCUSSION

Figure 2 shows SR-FWM data as a function of delay τ for an (electron-hole) excitation density $N=1\times10^{15}$ cm^{-3}, and clearly illustrates the apparent violation of the uncertainty principle. Note that N is always much larger ($\sim100x$) than the density of excitons. There is no detectable emission at the excitation energy (1.46 eV). Rather, the coherent emission is centered at the exciton energy and is approximately 1 meV wide. The spectral resolution is only 1.3 meV, so the width and spectral profile cannot be determined precisely. A spectral width of 1 meV implies a dephasing time greater than 500 fs, but clearly no emission occurs for pulse separations greater than the 40-fs pulsewidth. Figure 3(a) shows the coherent emission for $N=5\times10^{16}$ cm^{-3}; Fig. 3(b) shows the same data as a contour plot. The exciton feature is similar to that observed at low density, but the spectral width is larger as expected. [The modulation structure that appears on the exciton peak as a function of time delay in Figs. 2 and 3(a) is not understood at this time.] There is also a contribution from the continuum states near the excitation energy; this will be discussed in detail below. The main point we wish to make here is that the exciton and continuum contributions do not have the same density dependence. We have verified that the continuum contribution scales as N^3, which is expected in the small signal (i.e., $\chi^{(3)}$) limit. The difference in density scaling of the exciton and continuum signals is related to differences in the diffraction mechanism for the two contributions.

The density dependence of the exciton emission was investigated in a low resolution SR-FWM experiment. The monochromator was tuned to the exciton energy (1.415 eV)

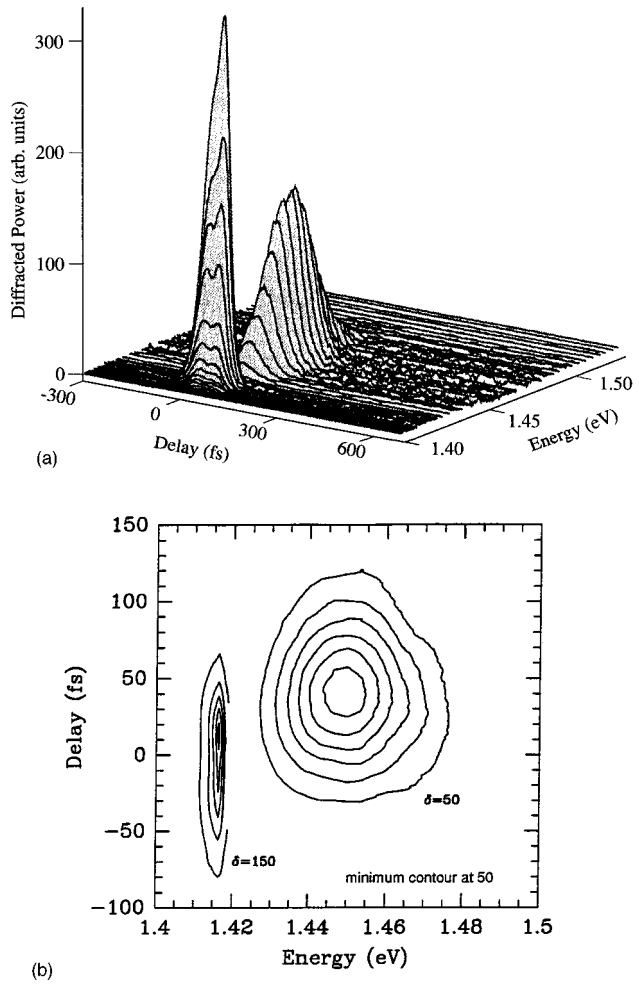

FIG. 3. (a) FWM spectrum vs delay for excitation at 1.46 eV and a carrier density of 5×10^{16} cm^{-3}. (b) Contour plot of the same data. The contour spacing δ is 50 units for the continuum peak at 1.45 eV, and 150 units for the exciton peak at 1.415 eV.

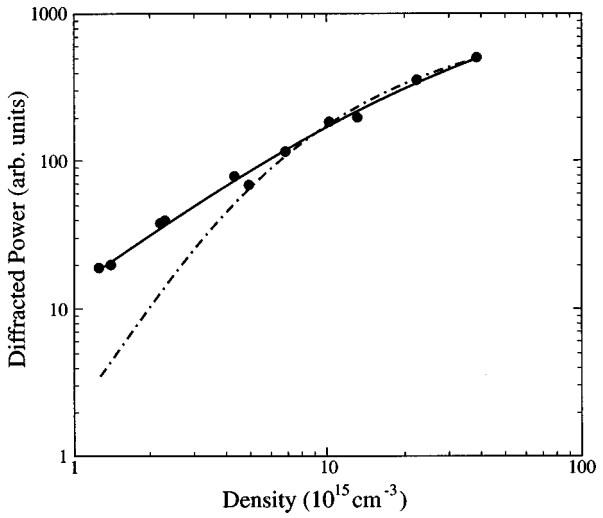

FIG. 4. Total diffracted power at the exciton energy vs density (circle) for excitation at 1.47 eV. The solid curve is a fit to the model with $m=0.5$ [see Eq. (15)] and the dashed curve is a fit to the simple EID model ($m=1$).

and the resolution set to 13 meV, which allowed the entire exciton emission bandwidth to be detected while filtering out the continuum contribution. In Fig. 4, the integrated exciton emission is plotted versus N, and exhibits a nearly linear dependence. Clearly this is very different from a cubic dependence which is typical of FWM in the small signal limit.

The apparent violation of the uncertainty principle as illustrated in Figs. 2 and 3, has been reported in other semiconductors, and interpreted as a coupling of continuum and exciton polarizations.[13,14,5,17] However, the EID mechanism, which is based on incoherent exciton-carrier scattering, has been known to affect exciton dephasing since the work of Schultheis *et al.*[3] Below, where we concentrate on the density dependence of exciton FWM results, we offer an interpretation only in terms of an EID model.

A. EID model

A simple model of exciton EID due to exciton-carrier scattering was presented by Wehner, Steinbach, and Wegener[18] and Birkedal *et al.*[19] We use the same basic model but employ a different assumption for the density dependence of the exciton dephasing rate. Since the EID model is presented in detail elsewhere, we only outline it here. Furthermore our focus is on the free-carrier density dependence of the exciton FWM emission. The coherent dynamics of excitons and continuum excitations are calculated with the SBE assuming no coherent interactions between excitons and continuum states. In an exciton basis, the dynamical equations for the exciton polarization P_x and occupation f_x are[20]

$$\left(\frac{\partial}{\partial t}+i\nu_x+\gamma_x\right)P_x\equiv i(1-2f_x)\frac{\mu_x E(t)}{\hbar}, \tag{1}$$

$$\frac{\partial}{\partial t}f_x\equiv -i\left(\frac{\mu_x E(t)}{\hbar}P_x^*-\frac{\mu_x E^*(t)}{\hbar}P_x\right), \tag{2}$$

where μ_x is the exciton dipole moment, ν_x is the detuning frequency, γ_x is the dephasing rate, and $E(t)$ is the component of the electric field of the optical pulse which drives the exciton. Equations (1) and (2) adequately describe many coherent effects such as Rabi flopping and free-induction decay, and can be extended to include such many-body effects as local-field corrections and exciton-exciton scattering. The excitation conditions of our experiments were specifically chosen to generate an exciton density which is low compared to that of free carriers. Under these conditions the free-induction decay contribution to the exciton FWM signal is negligible and exciton-exciton local-field effects are small, unlike the situation where excitons are resonantly excited in quantum wells.[30] The macroscopic polarization associated with the large bandwidth of excited continuum states is also short lived compared to the exciton dephasing time, so that continuum-induced local-field effects should also be small. In this regard we note that when the laser is tuned to 1.49 eV, with a substantially reduced overlap of the laser bandwidth with the exciton peak than that associated with Fig. 2, the exciton FWM signal drops by >50 times, indicating that coherent continuum-induced exciton excitation is negligible.[31] This apparently differs from the case of continuum-exciton coupling in a two-dimensional geometry.[17] For these reasons we neglect local-field corrections and exciton-exciton scattering in what follows.

The important features of the EID model are (i) the exciton dephasing rate is a function of excitation density, and (ii) the carrier density is spatially modulated. The phenomenological dephasing rate γ_x is assumed to depend on N, as a result of exciton-carrier scattering. Before we discuss our model for exciton-carrier scattering, we determine the N dependence of the EID mechanism under the assumption that γ_x varies linearly with N, i.e.,

$$\gamma_x = \gamma_0 + \Gamma_0 N. \tag{3}$$

The parameter Γ_0 is proportional to the exciton-carrier scattering cross section. The polarization amplitudes and $E(t)$ are taken to be slowly varying with a reference frequency equal to the exciton resonance frequency (i.e., $\nu_x = 0$, but this does not imply resonant excitation of the exciton). We take $f_x \ll 1$, since the sample is excited well above the exciton resonance. Therefore, the dynamics of f_x are not calculated, and f_x is taken to be zero for all time. The dynamical equation for P_x is, therefore

$$\left(\frac{\partial}{\partial t} + \gamma_0 + \Gamma_0 N\right) P_x \equiv i \frac{\mu_x E(t)}{\hbar}. \tag{4}$$

A dynamical equation for N is required to complete the model, and is derived from the coherent dynamics of the continuum states. A set of equations similar to Eqs. (1) and (2) is used to calculate the polarization and occupation for each continuum state (labeled by k). The energy of a continuum state is denoted by the detuning $\nu_k = E_b + \hbar^2 k^2 / 2m_r$, where E_b is the exciton binding energy and m_r is the electron-hole reduced mass. Since the exciton dephasing rate is assumed to be a function only of N, the details of the distribution function f_k are unimportant. Therefore, a detailed calculation of carrier scattering and cooling is not necessary. For simplicity the phenomenological continuum dephasing rate γ_k is assumed to be independent of k (over the bandwidth of the excitation). The free-carrier density $N = \Sigma_{\mathbf{k}} f_k$.

The model of coherent dynamics is applied to the FWM experimental geometry by employing a spatial Fourier transform of the exciton polarizations, carrier density and electric field.[20] For first-order diffraction, the spatial expansion can be restricted to the following terms:

$$E(t) = E_1(t+\tau) e^{i\mathbf{K}_1 \cdot \mathbf{r}} + E_2(t) e^{i\mathbf{K}_2 \cdot \mathbf{r}}, \tag{5}$$

$$P_x \equiv P_x^{(1)} e^{i\mathbf{K}_1 \cdot \mathbf{r}} + P_x^{(-1)} e^{i\mathbf{K}_2 \cdot \mathbf{r}} + P_x^{(3)} e^{i(2\mathbf{K}_1 - \mathbf{K}_2)\cdot \mathbf{r}} + P_x^{(-3)} e^{i(2\mathbf{K}_2 - \mathbf{K}_1)\cdot \mathbf{r}}, \tag{6}$$

$$f_k = f_k^{(0)} + f_k^{(2)} e^{i(\mathbf{K}_1 - \mathbf{K}_2)\cdot \mathbf{r}} + f_k^{(-2)} e^{i(\mathbf{K}_2 - \mathbf{K}_1)\cdot \mathbf{r}}, \tag{7}$$

$$N = N^{(0)} + N^{(2)} e^{i(\mathbf{K}_1 - \mathbf{K}_2)\cdot \mathbf{r}} + N^{(-2)} e^{i(\mathbf{K}_2 - \mathbf{K}_1)\cdot \mathbf{r}}. \tag{8}$$

The component of the exciton polarization that propagates into the diffracted direction $2\mathbf{K}_2 - \mathbf{K}_1$ is $P_x^{(-3)}$ and is coupled only to the component $P_x^{(-1)}$ in this model. By substituting these spatial Fourier transforms into Eq. (4), the EID diffraction mechanism becomes clear. It should be emphasized that since we have assumed no coherent interaction between excitons and free carriers, N can be determined independently of P_x. The distribution of free carriers is therefore part of the excitons' environment, and contributes to dephasing.

Analytic expressions can be obtained by assuming the excitation pulses are short compared to the dephasing time, and can be approximated as δ functions, i.e., $E_1(t) = A_1 \delta(t+\tau)$ and $E_2(t) = A_2 \delta(t)$. The dominant terms in the rate equation for $P_x^{(-1)}$ are

$$\frac{\partial}{\partial t} P_x^{(-1)} = i \frac{\mu_x A_2}{\hbar} \delta(t) - (\gamma_0 + \Gamma_0 N^{(0)}) P_x^{(-1)}, \tag{9}$$

which assumes that the amount of power diffracted is small compared to the amount transmitted (i.e., $P_x^{(-1)} \gg P_x^{(-3)}$). The solution of the rate equation for $P_x^{(-3)}$ is

$$P_x^{(-3)}(t) = \Gamma_0 N^{(-2)} \frac{\mu_x A_2}{\hbar} t e^{-(\gamma_0 + \Gamma_0 N^{(0)})t} \Theta(t), \tag{10}$$

where $\Theta(t)$ is the Heaviside function. The diffracting exciton polarization increases in time initially and then decays with a time constant determined by the dephasing rate. The emission spectrum due to EID is obtained by a Fourier transform and has a squared Lorentzian profile.[21] The total diffracted power J at the exciton energy due to EID is given by

$$J \propto \int_0^\infty |\mu_x P_x^{(-3)}(t)|^2 dt, \tag{11}$$

yielding

$$J \propto \frac{1}{4} \frac{(\Gamma_0 N^{(-2)})^2 A_2^2 \mu_x^4}{(\gamma_0 + \Gamma_0 N^{(0)})^3}. \tag{12}$$

Thus J is not a simple function of density (with $A_1 = A_2$ corresponding to our experimental situation; note that $N^{(\pm 2)} = N^{(0)}$) even though a simple approximation was used for the exciton scattering rate in Eq. (3). In some respects this result is unexpected because the EID term contained within Eq. (4) is proportional to E^3 and one would expect $J \propto (N^{(-2)})^3$. However, the temporal behavior of $P_x^{(-3)}(t)$ is not so easily seen from Eq. (4). The density dependence in Eq. (12) results from the fact that diffracting polarization density must be ''burned into'' the exciton polarization density over time [see Eq. (10)].

The dependence of J on delay τ is determined by solving the rate equation for $N^{(-2)}$. From Ref. 21 we obtain

$$f_k^{(-2)} = \mu_k^2 A_1 A_2 e^{-i(E_g - E_b + \nu_k)\tau} e^{-\gamma_k \tau} [\Theta(\tau)\Theta(t-\tau) + \Theta(-\tau)\Theta(t)], \tag{13}$$

which then gives

$$N^{(-2)} = \sum_k f_k^{(-2)} = \mu_k^2 A_1 A_2 e^{-\gamma_k \tau} \Theta(t) \delta(\tau). \tag{14}$$

Thus the EID mechanism is only operative for pulses which possess some temporal overlap. Since a density grating is required for the EID mechanism, the two pulses cannot be orthogonally polarized. The exciton scattering rate is assumed to depend only on carrier density and not on the carrier's angular momentum.

Figure 4 shows a fit of Eq. (12) to the experimental data. A linear dependence of the scattering rate with N gives poor agreement at low N. However, as was done by Becker *et al.*,[24] for free carriers we now consider that over the density range of interest to us γ_x has the functional dependence:

$$\gamma_x = \gamma_0 + \alpha N^m = \gamma_0 + \Gamma(N), \quad 0 < m < 1. \tag{15}$$

In this case Γ has spatial Fourier components, since N does [see Eq. (8)], with

$$\Gamma = \Gamma^{(0)} + \Gamma^{(2)} e^{i(\mathbf{K}_1 - \mathbf{K}_2)\cdot \mathbf{r}} + \Gamma^{(-2)} e^{i(\mathbf{K}_2 - \mathbf{K}_1)\cdot \mathbf{r}}, \tag{16}$$

and the expression for exciton FWM must be modified to

$$J \propto \frac{1}{4} \frac{(\Gamma^{(-2)})^2 A_2^2 \mu_x^4}{(\gamma_0 + \Gamma^{(0)})^3}, \tag{17}$$

with

$$\Gamma^{(-2)} = \frac{1}{\text{vol}} \int \Gamma(N) e^{-i(\mathbf{K}_2 - \mathbf{K}_1)\cdot \mathbf{r}} d\mathbf{r}, \tag{18}$$

where the integral is taken over the excitation volume (vol). As noted following Eq. (12), for light pulses with the same amplitude the spatial modulation of $N(=N^{(\pm 2)})$ is the average value of $N(=N^{(0)})$. From Eqs. (8) and (18) and for $m = 0.5$, we obtain $\Gamma^{(-2)} \propto \sqrt{N^{(0)}}$. Excellent agreement between the experiment and calculation is indeed obtained for this m value (± 0.05), for which the exciton-carrier scattering rate scales as $\sqrt{N}$. We now consider possible origins of such a density dependence.

The scattering rate for an exciton interacting with free carriers depends on the strength of the screened Coulomb (monopole-dipole) interaction and the occupany of final scattering states for the carriers.[32] In the low-density (below that considered here) and high-carrier temperature regime one can ignore phase-space filling and screening effects of the carriers and obtain that the total scattering rate is proportional to N. This underlies the basis for EID mechanisms considered by others. As the carrier density increases one might expect to observe a deviation from this behavior for one or more of the following reasons: (i) a Fermi distribution replaces a Boltzmann distribution for f_k; (ii) phase-space filling becomes important as $(1\text{-}f_k)$ approaches zero; and (iii) the interaction matrix element is a function of density because the Coulomb interaction is screened. Immediately after excitation $f_k \ll 1$ [the electrons (holes) are injected with $>$40- (10-) meV *average* excess energy] and most likely remains small during most of the exciton coherence time since the most effective mechanism for carrier cooling, *viz.* LO-phonon emission, can only influence carriers with greater energy (see the remarks on continuum dephasing below). We therefore anticipate that screening of carrier-exciton interactions will be the most important effect and lead to a sublinear dependence of scattering rate on density. A $N^{0.3}$ variation of the screened nonequilibrium carrier-carrier scattering rate was deduced by Becker *et al.*,[24] and substantiated by Young *et al.*[33] A complete picture of the screened carrier-exciton interaction would be more difficult to achieve since it is highly dependent on the dynamics of the screening process and details of the evolving nonequilibrium carrier densities.[1] Finally, our densities are also sufficiently high (the intercarrier separation is as low as 20 nm, comparable to the exciton diameter) that one might also expect a density dependence of the exciton oscillator strength through screening of the bound electron-hole interaction. This would affect the variation of J with N. Our experimental results do not permit a determination of the relative contributions of all the effects outlined here, and more extensive FWM experiments examining, e.g., temporally and spectrally resolved amplitude and phase of the FWM signal may have to be carried out.[30,34]

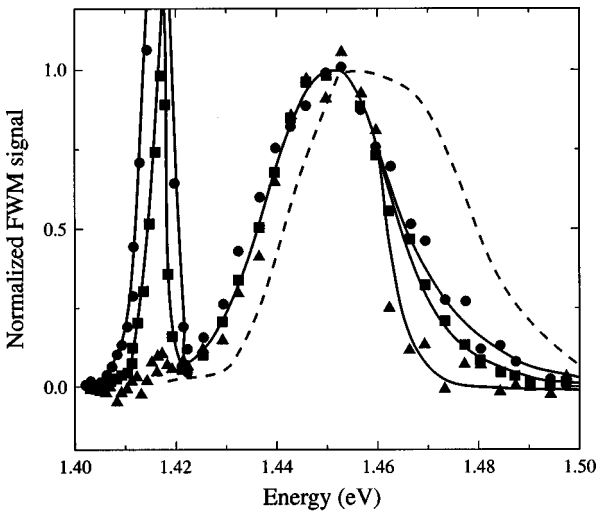

FIG. 5. FWM spectra at delays of -25 (circles), 25 (squares), and 100 fs (triangles) [cuts through the data shown in Fig. 3(b)]. The dashed curve is the laser spectrum and the other curves are guides to the eye.

Note also that the form of the density dependence of γ_x is only chosen for mathematical simplicty, and not meant to suggest a particular mechanism. However for an exciton-carrier scattering rate which scales as N^m, Eq. (16) allows the ratio α/γ_0 to be determined. For $m=1$ the ratio was determined to be 0.16×10^{-15} cm^3, (indicating that the exciton dephasing rate would have increased by a factor of ~ 8 over our density range), whereas with $m=0.5$ the ratio was determined to be $0.89 \times (10^{-15}$ cm$^3)^{0.5}$ (indicating a factor of ~ 4 increase). The spectral resolution was too low to determine the exciton dephasing rate accurately at low density.

B. Continuum dephasing

The dephasing rate of continuum states near the band edge was investigated by analyzing the SR-FWM data shown in Fig. 3. The peak of the continuum emission clearly occurs at a later delay than the peak of the exciton emission because the two signals arise from different diffraction mechanisms, EID in the case of the exciton emission, and a photon echo emission in the case of the continuum.[2] The feature we wish to call attention to here is the distortion of the contours at high energy and long delay times. The evolution of the FWM spectrum is shown more clearly by spectral cuts through the SR-FWM surface at delays $\tau = -25$, 25, and 100 fs which are shown in Fig. 5 along with the laser spectrum. All spectra have been normalized to unity at the peak of the continuum emission for ease of comparison. It

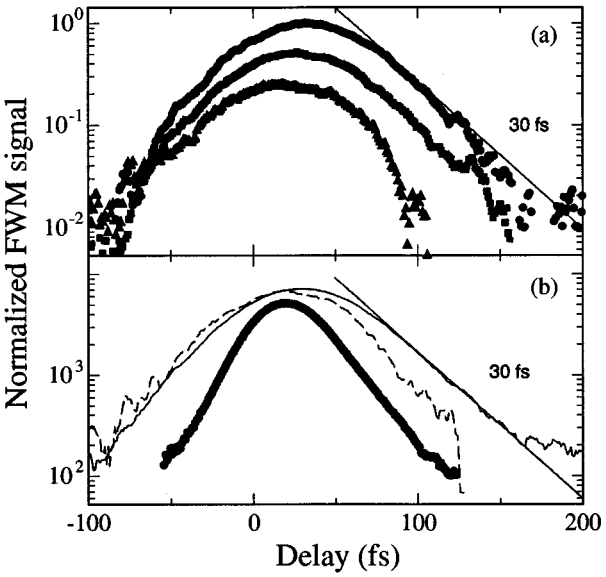

FIG. 6. (a) FWM signal vs delay for three detection energies [cuts through the data shown in Fig. 3(b)]; from top to bottom the energies are 1.455, 1.435, and 1.475 eV. The solid line represents a 30-fs decay constant. In (b) the numerically integrated FWM spectrum for two energy ranges (solid curve is for energies below 1.46 eV and the dashed curve is for energies above 1.46 eV) is shown vs delay. The SI-FWM signal using 1.51-eV pulses is indicated by the series of solid dots.

should be pointed out that the shift of the emission spectrum to lower energy than the excitation spectrum is the result of larger interband polarizability (Coulomb enhancement[35]) at lower energies. Its effect is largest near the band edge. Erland *et al.*[36] showed that the FWM spectrum from an inhomogeneously broadened transition can become distorted for long delays due to interference of different frequency components. However, we have verified by calculation that for our case the FWM spectrum would be symmetric about the peak of emission for all delays. If the dephasing rate were constant over the entire energy range, the spectra would not change shape so dramatically at a long delay. Since the spectra become asymmetric as the delay increases, the distortion is attributed to faster dephasing of continuum excitations above 1.46 eV. To estimate the average carrier energies, band-gap renormalization (BGR) must be taken into account. The BGR is estimated[37] to be ~ 7 meV. Therefore, electrons excited from the heavy-hole (HH) band have an energy of 41 meV and the hole energies are 6 (HH) and 19 meV (light-hole). The plasmon energy for $N=5\times10^{16}$ cm^{-3} is ~ 8 meV, too small to account for the increased dephasing rate above 1.46 eV. The LO- and TO-phonon energies are 41 and 38 meV, but TO-phonon emission is symmetry forbidden for electrons near the center of the Brillouin zone (Γ valley). Since the holes do not have enough energy to emit TO or LO phonons, the increased dephasing rate is attributed to LO-phonon emission by electrons.

From the decay of the emission versus delay, the polarization dephasing rate can be estimated. Temporal slices through the diffraction surface for 1.435, 1.455, and 1.475 eV are shown in Fig. 6(a). Clearly the decay is very rapid for all energies. However, decay constants should only be extracted from spectrally integrated measurements, since spectrally resolved results can be affected by interference effects. The SR-FWM results were numerically integrated, from the band edge up to 1.46 eV and from 1.46 eV to the high-energy extreme of the spectrum, to analyze the decay constants above and below the threshold energy. The results are shown in Fig. 6(b). To minimize the effect of pulse width convolution, the decay constant is extracted from the data for delay $t>100$ fs. For $\hbar\omega_s<1.46$ eV, the echo decay time is 30 fs, which is close to the resolution limit with 50-fs pulses (the leading edge of the echo has a 22-fs rise time). A line with a 30-fs decay constant is shown in Fig. 6(a) for comparison to the SR data, which are affected slightly by interference. Since the emission is a photon echo, a 33-ps^{-1} decay constant corresponds to a polarization dephasing rate of $\frac{1}{4}$, the echo decay rate, or $\gamma_k\sim 8$ ps^{-1}. Because the echo decay time constant is comparable to the pulse width we have assessed the influence of pulse width on the decay constant. In particular the SBE were used for a distribution of electron-hole pair states with an energy distribution quadratic in the wave vector **k**. Calculations were performed using 1000 points in **k** space from zero to 500 μm^{-1} in 1-fs steps up to 1 ps. The pulse intensity was assumed to have a sech^2 temporal profile with full width at half maximum of τ_p. The pulse width and dephasing rate were varied to optimize agreement with the experimental results. By inspection, the optimal parameters were determined to be $\tau_p=55\pm5$ fs and $\gamma_k=12\pm2$ ps^{-1}. The numerical results indicate that the echo decay rate may be larger than the 33 ps^{-1} derived directly from the data. The decay rate for the trace above 1.46 eV is not resolved from the pulse profile, and therefore a phonon emission rate cannot be obtained directly from a comparison of the dephasing rates above and below the threshold energy. This is mainly due to the noise level rather than the bandwidth of the pulses; at $\tau=100$ fs the signal is essentially at the noise level.

The value of the dephasing rate is not the significant result here. More important is the fact that the dephasing rate is observed to change abruptly in SR-FWM below a threshold of 1.46 eV, and that this threshold is clearly related to the onset of LO-phonon emission by electrons. The $\sim$33-ps^{-1} decay constant cannot be entirely ascribed to an artifact of the pulse shape and/or convolution effects. The continuum dephasing rate is therefore at least 8 ps^{-1} below the threshold for LO-phonon emission by electrons at a carrier density of $N=5\times10^{16}$ cm^{-3}. Dephasing rates for continuum excitations in bulk GaAs have been reported at similar excess carrier energy and density. Wehner *et al.* measured a continuum dephasing rate of 20 ps^{-1} in GaAs by FWM with 15-fs pulses.[23] In other reports, continuum dephasing rates of 5 ps^{-1} were measured with 100-fs pulses.[15,27] At much higher photon energy and higher carrier density than the experiments reported here, the continuum dephasing rate in bulk GaAs was measured by FWM with 6-fs pulses[24] to be 25–50 ps^{-1}, and to be a function of carrier density. Continuum dephasing rates have also been measured from FWM experiments in modulation-doped quantum wells[25] and quantum-well structures.[26] Unfortunately these authors did not estimate the influence of pulse convolution effects on the continuum dephasing rate.

Since the dephasing rate above the LO-phonon emission threshold was not resolved with 50-fs pulses and SR-FWM detection, an attempt was made to resolve the decay with SI-FWM and shorter pulses at higher energy. SI-FWM experiments were performed with 30 fs pulses centered[31] at 1.51 eV at a density $N=8\times10^{16}$ cm^{-3}, and are shown in Fig. 6(b). The decay rate of the SI-FWM trace is 50 ps^{-1}, implying a continuum dephasing rate >13 ps^{-1}. Therefore, the LO-phonon emission rate is estimated to be at least 5 ps^{-1}. The LO-phonon emission rate in InP is calculated to be 10 ps^{-1} using the expression for polar-optical-phonon scattering,[38] and a value in the range 14–20 ps^{-1} has been estimated from photoemission experiments.[39]

Finally, Fig. 3(b) clearly indicates that continuum emission peaks at earlier times for lower energies and approaches that associated with the exciton emission. This trend has been verified over a broad range of densities. Since EID emission peaks at zero delay (this defines when the density grating amplitude is maximum) while the photon echo response is characterized by a delayed peak,[2] our result may offer evidence of EID contributions from continuum states near the band edge. This may not be entirely unexpected since a Coulomb enhancement of the absorption edge appears in linear optical processes for excess carrier energies of several meV. Further work will be carried out to investigate this aspect of coherent continuum dynamics.

IV. CONCLUSIONS

The coherent response of InP at 5 K has been investigated over a 140-meV range near and above the band gap, using spectrally resolved and spectrally integrated four-wave mixing with 30–50-fs pulses. For excitation near the band gap, excitons were excited simultaneously with a large bandwidth of continuum excitations. The emission from excitons is consistent with an excitation-induced dephasing mechanism. The dependence of the diffracted power on excitation density was shown to be nearly linear from 1×10^{15} to 5×10^{16} cm^{-3}, and not cubic as would be the case for free-induction decay. A simple model of coherent exciton dynamics based on a square-root dependence of the exciton dephasing rate on carrier density was shown to explain the results over a wide density range.

The coherent dynamics of continuum excitations associated with the light- and heavy-hole valence bands and the electron conduction band were investigated from the band edge up to 140 meV above the band gap. The continuum dephasing rate increases abruptly at the threshold energy for LO-phonon emission by electrons. Below this threshold energy, the dephasing rate was determined to be ~8 ps^{-1} at a density of 5×10^{16} cm^{-3}. Above the threshold energy, the dephasing rate was not resolved at this density with 50-fs pulses. By using perpendicularly polarized 30-fs pulses and spectrally integrated detection, the dephasing rate was estimated to be at least 13 ps^{-1} for the continuum states above the phonon emission threshold. This is the first report of an increased continuum dephasing rate associated with LO-phonon emission.

ACKNOWLEDGMENTS

We gratefully acknowledge financial support from the Natural Sciences and Engineering Research Council of Canada and Photonics Research Ontario. H.M.vD. acknowledges support from the Killam Program of the Canada Council. We have also benefited from helpful discussions with S.T. Cundiff, J.F. Young, and K.C. Hall.

[1] H. Haug and S. W. Koch, *Quantum Theory of the Optical and Electronic Properties of Semiconductors* (World Scientific, NJ, 1994).
[2] J. Shah, *Ultrafast Spectroscopy of Semiconductors and Semiconductor Nanostructures* (Springer, Berlin, 1996).
[3] L. Schultheis, J. Kuhl, A. Honold, and C. W. Tu, Phys. Rev. Lett. **57**, 1635 (1986).
[4] M. Wegener, D. S. Chemla, S. Schmitt-Rink, and W. Schäfer, Phys. Rev. A **42**, 5675 (1990).
[5] K. Leo, M. Wegener, J. Shah, D. S. Chemla, E. O. Göbel, T. C. Damen, S. Schmidt-Rink, and W. Schäfer, Phys. Rev. Lett. **65**, 1340 (1990).
[6] S. Schmitt-Rink, S. Mukamel, K. Leo, J. Shah, and D. S. Chemla, Phys. Rev. A **44**, 2124 (1991).
[7] S. Weiss, M. A. Mycek, S. Schmitt-Rink, and D. S. Chemla, Phys. Rev. Lett. **69**, 2685 (1992).
[8] K. Bott, O. Heller, D. Bennhardt, S. T. Cundiff, P. Thomas, F. J. Mayer, G. O. Smith, R. Eccleston, J. Kuhl, and K. Ploog, Phys. Rev. B **48**, 17 418 (1993).
[9] T. Yajima and Y. Taira, J. Phys. Soc. Jpn. **47**, 1620 (1979).
[10] A. M. Weiner, S. D. Silvestri, and E. P. Ippen, J. Opt. Soc. Am. B **2**, 654 (1985).
[11] J. Kuhl, A. Honold, L. Schultheis, and C. W. Tu, Adv. Solid State Phys. **29**, 157 (1989).
[12] E. O. Göbel, Adv. Solid State Phys. **30**, 269 (1990).
[13] T. Rappen, U. Peter, M. Wegener, and W. Schafer, Phys. Rev. B **48**, 4879 (1993).
[14] T. Rappen, U.-G. Peter, M. Wegener, and W. Schäfer, Phys. Rev. B **49**, 10 774 (1994).
[15] A. Leitenstorfer, A. Lohner, K. Rick, P. Leisching, T. Elsaesser, T. Kuhn, F. Rossi, W. Stolz, and K. Ploog, Phys. Rev. B **49**, 16 372 (1994).
[16] D. S. Kim, J. Shah, J. E. Cunningham, T. C. Damen, W. Schäfer, M. Hartmann, and S. Schmidt-Rink, Phys. Rev. Lett. **68**, 1006 (1992).
[17] S. T. Cundiff, M. Koch, W. H. Knox, J. Shah, and W. Stolz, Phys. Rev. Lett. **77**, 1107 (1996).
[18] M. U. Wehner, D. Steinbach, and M. Wegener, Phys. Rev. B **54**, R5211 (1996).
[19] D. Birkedal, V. G. Lyssenko, J. M. Hvam, and K. El Sayed, Phys. Rev. B **54**, R14 250 (1996).
[20] M. Lindberg, R. Binder, and S. W. Koch, Phys. Rev. A **45**, 1865 (1992).
[21] H. Wang, K. Ferrio, D. G. Steel, Y. Z. Hu, R. Binder, and S. W. Koch, Phys. Rev. Lett. **71**, 1261 (1993).
[22] K. El Sayed, D. Birkedal, V. G. Lyssenko, and J. M. Hvam, Phys. Rev. B **55**, 2456 (1997).

[23] M. U. Wehner, D. Steinbach, M. Wegener, T. Marschner, and W. Stolz, J. Opt. Soc. Am. B **13**, 977 (1996).
[24] P. C. Becker, H. L. Fragnito, C. H. Brito Cruz, R. L. Fork, J. E. Cunningham, J. E. Henry, and C. V. Shank, Phys. Rev. Lett. **61**, 1647 (1988).
[25] D. S. Kim, J. Shah, J. E. Cunningham, and T. C. Damen, Phys. Rev. Lett. **68**, 2838 (1992).
[26] J.-Y. Bigot, M. Portella, R. W. Schoenlein, J. E. Cunningham, and C. V. Shank, Phys. Rev. Lett. **67**, 636 (1991).
[27] A. Lohner, K. Rick, P. Leisching, A. Leitenstorfer, T. Elsaesser, T. Kuhn, F. Rossi, and W. Stolz, Phys. Rev. Lett. **71**, 77 (1993).
[28] G. Augustine, N. M. Jokerst, and A. Rohatgi, Appl. Phys. Lett. **61**, 1429 (1992).
[29] See, e.g., *Semiconductors, Physics of Group IV Elements and III-V Compounds*, edited by O. Madelung, Landolt-Börnstein, New Series, Group III, Vol. 17, Pt. a (Springer-Verlag, Berlin, 1982); *Semiconductors Intrinsic Properties of Group IV Elements and III-V, II-VI, and I-VIII Compounds*, edited by O. Madelung, Landolt-Börnstein, New Series, Group III, Vol. 22, Pt. a (Springer-Verlag, Berlin, 1987), Chap. 2.13.
[30] S. Patkar, A. E. Paul, W. Sha, J. A. Bolber, and A. L. Smirl, Phys. Rev. B **51**, 10 789 (1995).
[31] G. R. Allan, Ph.D. thesis, University of Toronto, 1997.
[32] H. Haug, Z. Phys. B **24**, 351 (1976).
[33] J. F. Young, T. Gong, P. M. Fauchet, and P. J. Kelly, Phys. Rev. B **50**, 2208 (1994).
[34] W. J. Walecki, D. N. Fittinghof, A. L. Smirl, and R. Trebino, Opt. Lett. **22**, 81 (1997).
[35] H. Haug and S. Schmitt-Rink, J. Opt. Soc. Am. B **2**, 1135 (1985).
[36] J. Erland, K.-H. Pantke, V. Mizeikis, V. G. Lyssenko, and J. M. Hvam, Phys. Rev. B **50**, 15 047 (1994).
[37] R. Zimmermann, Phys. Status Solidi B **146**, 371 (1988).
[38] A. Nagy, in *Semiconductors Probed by Ultrafast Laser Spectroscopy*, edited by R. R. Alfano (Academic Press, Orlando, 1984), p. 3.
[39] J. Peretti, H.-J. Drouhin, and D. Paget, Phys. Rev. B **47**, 3603 (1993).